Progress In Electromagnetics Research C, Vol. 51, 111–119, 2014

Analytical Computation of AC Resistance of Single-Layer Air-Core Helmholtz Coils

Weijie Luo*, Quan Ke, Guozheng Yan, and Kai Yang

Abstract—An analytical expression of AC resistance of a single-layer air-core Helmholtz coil is presented. Proximity effects between both bundles and strands of litz-wire as well as skin effect are considered. To obtain an accurate analytical expression of proximity effect on bundle level and strand level, a precise distribution of magnetic field is discussed. The analytical expression of AC resistance and quality factor is verified with the experimental results, and the theoretical predictions are in agreement with the measured results.

1. INTRODUCTION

Power supply has been a major issue for micro medical devices that cannot use a cable to obtain energy. In this case, battery is a possible solution. However, batteries' limited storage capacity will not allow medical devices to work at a comparatively high power for a long period of time. For instance, most commercial wireless capsular endoscopic (WCE) devices used in gastrointestinal (GI) tract use batteries as their power supply. Latest WCE devices, which are capable of taking 2 or 3 frames of GI tract image per second and transmitting them to a receiver, can work for about 8–12 hours. Those batteries can provide an average of 25 mW of power, which is insufficient for capsule endoscopy that requires more power — capsule robots. Many efforts have been devoted to the development of a continuous power supply system [1], among which wireless power transfer (WPT) [2–5] is a promising option. This system can provide a steady and sufficient supply of energy to an endoscopy capsule.

WPT system consists of three components: (1) a driving circuit which can provide a square wave current; (2) a power transmitting coil; (3) a power receiving coil with a rectifier and filter circuit. In this wireless power transmission system for WCE devices, the diameter of the transmitting coil should be over 400 mm, which is bigger than most people's torsos, and that of the receiving coil should be no more than 15 mm, which is the minimum diameter of GI tract. Due to the great disparity between transmitting and receiving coil, a loosely coupled transformer with a large air gap in between is formed. The receiving coil affects the transmitting coil less as the diameter of the transmitting coil increases. In the meanwhile, the winding resistance of the transmitting coils becomes more significant. Thus it is necessary to analyze winding losses in transmitting coils at high frequency. The winding AC power loss of the coil at high frequency is caused by eddy currents, due to skin effect and proximity effect. Both effects will become more dominated as the frequency increases.

Litz-wire is commonly used to reduce winding power losses of inductors and transformers. Since litz-wire is multi-stranded, the overall current is distributed into each strand, which will result in a more uniform current distribution across the wire cross section. Besides, litz-wire is also twisted so that every strand can cover all the positions in the wire cross section along the longitudinal axis, and this property will make sure that current in each strand is the same. Therefore, not only the skin effect

Received 28 April 2014, Accepted 18 June 2014, Scheduled 23 June 2014

* Corresponding author: Weijie Luo (bozailaw@126.com).

The authors are with the Department of Instrument Science and Engineering, School of Electronic Information and Electrical Engineering, Shanghai Jiao Tong University, Shanghai 200240, China.

but also proximity effect is reduced [6]. In the following analysis, it is assumed that current density distribution is absolutely uniform in every strand.

Many approaches to analytical computation of AC resistance of multi-strand and litz-wire windings have been presented [6–11]. However, most of the analytical modelsare developed to calculate AC resistance of windings of inductors and transformers. Therefore these models have been derived under the following assumptions:

1) The core material has a high magnetic permeability.
2) The winding layer wires fill the entire breadth of the bobbin.

Under these two assumptions, the behavior of the winding is close to that of an ideally infinite long solenoid winding. But when analyzing the single-layer air-core Helmholtz coil that is used as power transmitting coil, those assumptions is invalid, for this coil does not have a high-permeability core and there is a huge air gap in the middle of the winding.

The purpose of this paper is to develop an analytical expression of AC resistance of a single-layer air-core Helmholtz coil. In the analysis, the magnetic field distribution across every conductor and every strand is considered. The influence of twisting of the litz-wire is also taken into account. The theoretical prediction is verified with experimental results.

Notation:

δ	Skin depth.
d_c	Diameter of a conductor.
d_0	Diameter of a strand.
H	Amplitude of the magnetic field.
f	Frequency.
N_0	Number of strands in a conductor.
N_T	Number of turns.
R_{ac}	AC resistance of the winding
ρ	Copper resistivity.
ζ	Normalized value of the diameter of a strand (d_0/δ).
I	Amplitude of current in conductors.
I_0	Amplitude of the current in strands.
p	Pitch of the twisting.
D	Diameter of the coil.
D_g	Length of air gap in the middle of the Helmholtz coil.

2. ANALYSIS OF THE MAGNETIC FIELD DISTRIBUTION ACROSS A LITZ-WIRE WINDING SPACE

Figure 1 shows the Helmholtz coil discussed in this paper. It consists of two identical solenoid coils with $N_T/2$ turns (N_T is even). The distance between these two solenoid coils is $D_g + \frac{N_T}{2} \times d_c = D/2$. Because the diameter of both solenoid coils R is much greater than the length of them $d_c N_T/2$, each solenoid coil should be considered as a row of $N_T/2$ ring coils in order to analyze the magnetic field. The external magnetic field across each turn (H_{ext}) is the accumulation of magnetic field generated by all other turns. Each turn is considered as a current ring, thus external magnetic field distribution across each turn (H_{ext}) can be derived by using Biot-Savart's law:

$$d\vec{H} = \frac{1}{4\pi} \frac{Id\vec{l} \times \vec{r}_p}{r_p^3} = \frac{1}{4\pi} \frac{Id\vec{l} \times (\vec{r}_0 - \vec{R})}{r_p^3} = \frac{IR}{4\pi r_p^3} \left[z\cos\theta \vec{i} + z\sin\theta \vec{j} + (R - x\cos\theta)\vec{k} \right] d\theta \tag{1}$$

Due to the symmetry of the ring current, as shown in Fig. 2, magnetic field at $P(x, 0, z)$ can represent magnetic field at any point in the space and magnetic field along y direction is 0 at P ($H_y = 0$). The

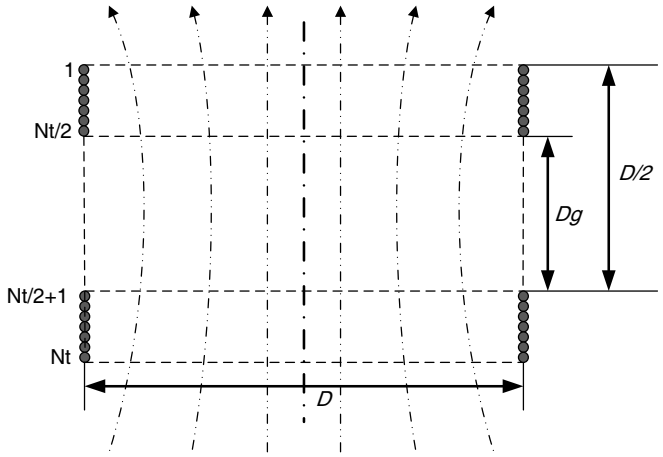

Figure 1. Single-layer air-core Helmholtz coil.

magnetic field at P is given by

$$H_x(x,z) = \int dH_x = \int_0^{2\pi} \frac{IR}{4\pi r_p^3(x,z)} z\cos\theta d\theta \tag{2}$$

$$H_z(x,z) = \int dH_z = \int_0^{2\pi} \frac{IR}{4\pi r_p^3(x,z)} (R - x\cos\theta) d\theta \tag{3}$$

where $r_p(x,z) = \sqrt{x^2+z^2+R^2-2Rx\cos\theta}$ and R is the radius of the coil.

Therefore, the magnetic field generated by the jth turn at the (r,φ) position of the ith turn is:

$$H_{xij}(r,\varphi) = H_x(R + r\sin\varphi, z_{ij} + r\cos\varphi) \tag{4}$$

$$H_{zij}(r,\varphi) = H_z(R + r\sin\varphi, z_{ij} + r\cos\varphi) \tag{5}$$

where $z_{ij} = \begin{cases} (i-j)\,d_c, & i \le \frac{N_T}{2}, j \le \frac{N_T}{2} \text{ or } i > \frac{N_T}{2}, j > \frac{N_T}{2} \\ (i-j)\,d_c - D_g, & i \le \frac{N_T}{2}, j > \frac{N_T}{2} \\ (i-j)\,d_c + D_g, & i > \frac{N_T}{2}, j \le \frac{N_T}{2} \end{cases}$.

The total magnetic field in (r,φ) position of the ith turn is:

$$H_{xi}(r,\varphi) = \sum\nolimits_{j=1,j\neq i}^{N_T} H_{xij}(r,\varphi) \tag{6}$$

$$H_{zi}(r,\varphi) = \sum\nolimits_{j=1,j\neq i}^{N_T} H_{zij}(r,\varphi) \tag{7}$$

Thus the amplitude of magnetic field at (r,φ) is:

$$H_i(r\varphi) = \sqrt{H_{xi}^2(r,\varphi) + H_{zi}^2(r,\varphi)} \tag{8}$$

The mean amplitude of external magnetic field across the ith turn is:

$$H_{exti} = \frac{1}{\pi r_c^2} \int_0^{2\pi} \int_0^{r_c} H_i(r,\varphi) r dr d\varphi \tag{9}$$

Computation of the results in Fig. 3 is achieved by using numerical calculation functions of Matlab. Unlike magnetic field of infinite long solenoid coil, magnetic field across each turn differs greatly with that of other turns. As shown in Fig. 3, amplitude of magnetic field is the lowest at 14, 15 turns and 42, 43 turns, which are in the middle of two identical solenoid coils, and reaches the highest points at turns on the edges of the Helmholtz coil.

To simplify the calculation of AC resistance in the following section, the external magnetic field at each turn is considered as a constant field with the amplitude of H_{exti}.

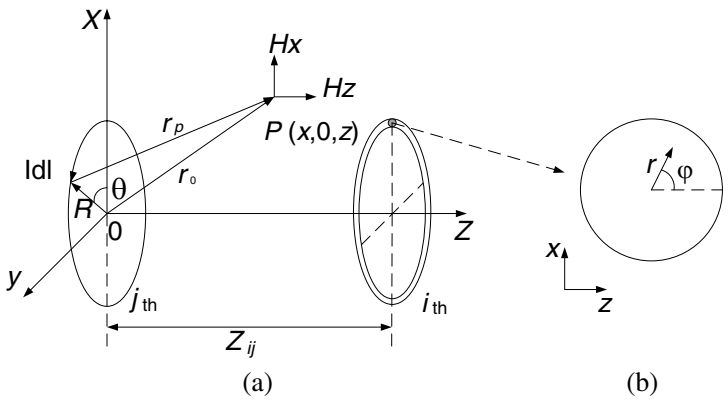

Figure 2. (a) Magnetic field generated by the jth current ring. (b) Cross section of the ith ring (in xz-plane).

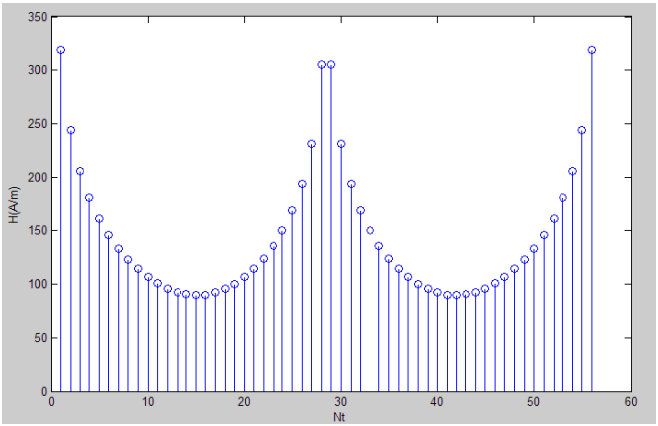

Figure 3. Calculated amplitude of magnetic field at each turn when $I = 1$ and $N_T = 56$.

Besides the external magnetic field in the winding (H_{ext}), each strand in a given conductor is also submitted to an internal magnetic field (H_{int}) that is generated by current in other strands in the same conductor, as shown in Fig. 4. Since all strands in this conductor is twisted, it is assumed that each strand has the same current, which is I/N_0.

Current vector of a single strand travels through a helix along the longitudinal axis of the conductor, as shown in Fig. 5. Considering that current vectors in all strands have similar paths, the internal magnetic field generated by them is not perpendicular to the cross section plane of this given conductor nor in the plane. The internal magnetic field can be divided into two components: one is the magnetic field perpendicular to the plane ($H_\perp$) and another one is the magnetic field in the cross section plane (H_p). In the following analysis, we suppose that current density at any position across the conductor has the same amplitude and slant angle.

As shown in Fig. 4, under the assumption that the current density distribution is uniform, the magnetic field in the cross section plane (H_p) can be given by

$$H_p(r) = \frac{I}{2\pi r_c^2} r \tag{10}$$

As shown in Fig. 5, current density J can be divided into two components: current density in the cross section plane (J_p) and current density perpendicular to the plane ($J_\perp$). $J_\perp$ points out of the front of the diagram, and J_p follows the counterclockwise direction, which is also the twisting direction of litz-wire.

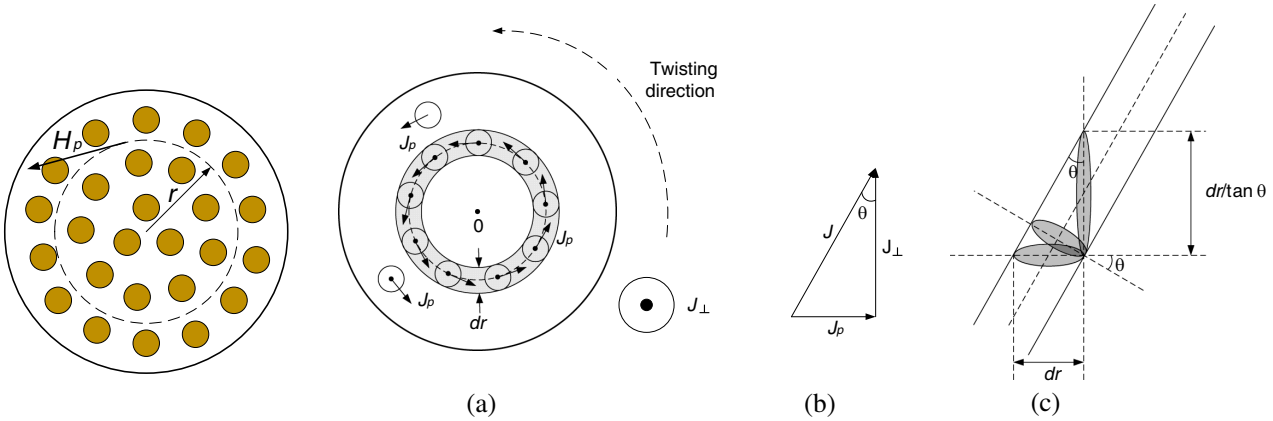

Figure 4. Cross section of a conductor.

Figure 5. (a) Two kinds of current density in a conductor: J_p and $J_\perp$. (b) Geometric relationship between J_p and $J_\perp$. (c) Cross section of different directions in a given strand.

The current density perpendicular to the plane $J_\perp$ is given by

$$J_\perp = \frac{I}{2\pi r_c^2} \tag{11}$$

$J_\perp$ and J_p is submitted to the geometrical relationship in Fig. 5(b):

$$J_p = J_\perp \tan\theta \tag{12}$$

where θ is the slant angle, $\tan\theta = \frac{2\pi r_c}{p}$, and p the pitch of the twisting.

Within the shaded ring area in Fig. 5(a), J_p is continuous. Therefore, this shaded ring is equivalent to a current ring. Since there are countless similar current rings with the same radius along the longitudinal axis of the conductor, the magnetic field generated by these current rings is identical to that of an ideally infinite long solenoid coil. The curvature of the wire is neglected because $d_c \ll D$.

Thus to obtain the magnetic field generated by J_p, which is $H_\perp$, we need the density of J_p along the longitudinal axis, as shown in Fig. 5(c):

$$n = \frac{\tan\theta}{dr} \tag{13}$$

The magnetic field generated by J_p at $r = R$ $(R < r_c)$ is

$$H_\perp(R) = \int_R^{r_c} nJ_p \times dr \times \frac{dr}{\tan\theta} = \frac{I}{2\pi r_c^2}\tan\theta(r_c - R) \tag{14}$$

Apparently, the direction of $H_\perp$ is parallel to the longitudinal axis.

The total internal magnetic field is

$$H_{int}(r) = \sqrt{H_p(r)^2 + H_\perp(r)^2} = \sqrt{\frac{I^2}{(2\pi r_c^2)^2}r^2 + \frac{I^2}{(2\pi r_c^2)^2}\tan^2\theta(r_c - r)^2} \tag{15}$$

3. AC RESISTANCE OF ROUND LITZ-WIRE WINDINGS

Eddy current losses per unit length in a strand of a given conductor (the ith turn) is [8]

$$P_0 = \frac{I_0^2\rho}{\sqrt{2}\pi\delta d_0}\psi_1(\zeta) - \frac{2\sqrt{2}\pi\rho}{\delta}H^2\psi_2(\zeta), \quad \zeta = \frac{d_0}{\delta}, \quad I_0 = \frac{I}{N_0}. \tag{16}$$

It is assumed that the external magnetic field across every turn is constant, thus proximity losses can be calculated as the sum of contributions due to the internal magnetic field (H_{int}) and to the external one (H_{ext}) [7]. Losses of a strand at the radius r of the conductor can be expressed as

$$P_0 = \frac{I_0^2\rho}{\sqrt{2}\pi\delta d_0}\psi_1(\zeta) - \frac{2\sqrt{2}\pi\rho}{\delta}\left(H_{int}^2(r) + H_{exti}^2\right)\psi_2(\zeta) \tag{17}$$

where

$$\begin{aligned}\psi_1(\zeta) &= \frac{ber(\zeta/\sqrt{2})bei'(\zeta/\sqrt{2}) - bei(\zeta/\sqrt{2})ber'(\zeta/\sqrt{2})}{[ber'(\zeta/\sqrt{2})]^2+[bei'(\zeta/\sqrt{2})]^2}\\ \psi_2(\zeta) &= \frac{ber_2(\zeta/\sqrt{2})ber'(\zeta/\sqrt{2}) + bei_2(\zeta/\sqrt{2})bei'(\zeta/\sqrt{2})}{[ber(\zeta/\sqrt{2})]^2+[bei(\zeta/\sqrt{2})]^2}\end{aligned} \tag{18}$$

$ber()$ and $bei()$ are the zeroth-order Kelvin functions, and $ber_2()$ and $bei_2()$ are the second-order Kelvin functions. $ber'()$ and $bei'()$ are the first derivatives of $ber()$ and $bei()$, respectively. These functions can be calculated by using Bessel function:

$$\begin{aligned}ber(x) &= \mathrm{Re}\left[J_0\left(xe^{\frac{3\pi i}{4}}\right)\right]\\ bei(x) &= \mathrm{Im}\left[J_0\left(xe^{\frac{3\pi i}{4}}\right)\right]\\ ber_2(x) &= \mathrm{Re}\left[J_2\left(xe^{\frac{3\pi i}{4}}\right)\right]\\ bei_2(x) &= \mathrm{Im}\left[J_2\left(xe^{\frac{3\pi i}{4}}\right)\right]\\ ber'(x) &= \frac{dber(x)}{dx} = \mathrm{Re}\left[\sqrt{2}\left(\frac{1}{2}-\frac{i}{2}\right)J_1\left(\sqrt{2}x\left(-\frac{1}{2}+\frac{i}{2}\right)\right)\right]\\ bei'(x) &= \frac{dber(x)}{dx} = \mathrm{Im}\left[\sqrt{2}(\frac{1}{2}-\frac{i}{2})J_1\left(\sqrt{2}x(-\frac{1}{2}+\frac{i}{2})\right)\right]\end{aligned} \tag{19}$$

where J_v is the vth-order Bessel function of the first kind.

The density of eddy current losses at the radius r of the ith turn conductor can be obtained by multiplying the eddy current losses density of a given strand at radius r, which is $\frac{P_0(r)}{\pi r_0^2}$ by packing factor $\beta = \frac{k\pi r_0^2}{\pi r_c^2} = \frac{kr_0^2}{r_c^2}$. Here packing factor β indicates the ratio of the total cross-sectional area of all strands in the conductor to the cross-sectional area of the whole conductor.

$$\frac{dP_i}{dS} = \frac{P_0(r)}{\pi r_0^2}\beta = \frac{I_0^2\rho\beta}{2\sqrt{2}\pi^2\delta r_0}\psi_1(\zeta) - \frac{2\sqrt{2}\rho\beta}{\delta r_0}\left(H_{int}^2(r) + H_{exti}^2\right)\psi_2(\zeta) \tag{20}$$

From (9), (15) and (20), we can obtain power loss per unit length in the given conductor by integrating the density of eddy current losses

$$P_i = \int_0^{2\pi}\int_0^{r_c}\frac{dP_i}{dS}rdrd\varphi = \frac{I^2\rho}{\sqrt{2}\pi\delta N_0 d_0}\psi_1(\zeta) - \frac{I^2\rho\beta}{\sqrt{2}\pi\delta d_0}\left(1+\frac{\tan^2\theta}{3}\right)\psi_2(\zeta) - \frac{4\sqrt{2}\pi\rho\beta I^2 r_c^2}{\delta d_0}\frac{H_{exti}^2}{I^2}\psi_2(\zeta) \tag{21}$$

Therefore, the power dissipation of the whole coil is the sum of power dissipation of all turns

$$P = \sum_{i=1}^{N_T} P_i l_T = \frac{I^2\rho N_T l_T}{\sqrt{2}\pi\delta N_0 d_0}\psi_1(\zeta) - \frac{I^2\rho\beta N_T l_T}{\sqrt{2}\pi\delta d_0}\left(1+\frac{\tan^2\theta}{3}\right)\psi_2(\zeta) - \frac{4\sqrt{2}\pi\rho\beta I^2 l_T r_c^2}{\delta d_0}\sum_{i=1}^{N_T}\frac{H_{exti}^2}{I^2}\psi_2(\zeta) \tag{22}$$

The AC resistance of the coil can be expressed by

$$R_{ac} = \frac{2P}{I^2} = \frac{\sqrt{2}\rho N_T l_T}{\pi\delta N_0 d_0}\psi_1(\zeta) - \frac{\sqrt{2}\rho\beta N_T l_T}{\pi\delta d_0}\left(1+\frac{\tan^2\theta}{3}\right)\psi_2(\zeta) - \frac{8\sqrt{2}\pi\rho\beta r_c^2 l_T}{\delta d_0}\sum_{i=1}^{N_T}\frac{H_{exti}^2}{I^2}\psi_2(\zeta) \tag{23}$$

4. EXPERIMENTAL RESULTS

Since it is impossible to measure AC resistance of a winding directly due to the influence introduced by stray-capacitance, a lumped-parameter equivalent circuit model of inductors is used [10], as shown in Fig. 6(a). L is the nominal inductance, R_{ac} the AC resistance, and C the stray-capacitance. Most LCR meters measure an equivalent series reactance X_s and an equivalent series resistance (ESR) R_s as shown in Fig. 6(b):

$$Z = \frac{R_{ac}}{\left(1-\omega^2 LC\right)^2 + \left(\omega C R_{ac}\right)^2} + j\omega L \frac{1-\omega^2 LC - CR_{ac}^2/L}{\left(1-\omega^2 LC\right)^2 + \left(\omega C R_{ac}\right)^2} = R_s + jX_s = |Z|\, e^{j\theta} \tag{24}$$

The quality factor of the coil is given by

$$Q = \frac{|X_s|}{R_s} = \frac{\left|\omega L(1-\omega^2 LC - CR_{ac}^2/L)\right|}{R_{ac}} \tag{25}$$

The stray-capacitance can be calculated by

$$C = \frac{1}{4\pi^2 f_{self}^2 L} \tag{26}$$

Tests were performed using a HIOKI 3532-50 LCR HITESTER equipped with a HIOKI 9262 test fixture. Two coils that were tested have a same radius of 380 mm. The first coil has 56 turns while the second has 20. The air gap in the middle of both Helmholtz coil is 327 mm. The diameter of litz-wire is 2 mm, and there are 180 strands in one bundle. Each strand has a diameter of 0.1 mm and the pitch of the litz-wire is 16 mm.

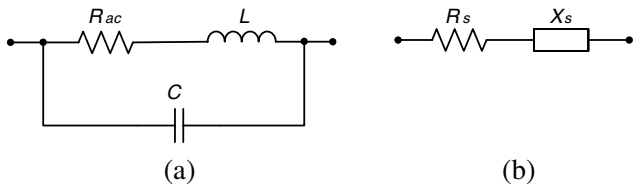

Figure 6. (a) Lumped-parameter equivalent circuit. (b) Equivalent series circuit.

The inductances and self-resonant frequencies of both coils is measured: $L_1 = 2.751$ mH, $L_2 = 0.448$ mH, $f_{self1} = 830$ kHz and $f_{self2} = 1907$ kHz. The self-resonant frequencies were measured at zero phase of the impedance.

Thus stray-capacitance can be calculated using (26): $C_1 = 13.36$ pF and $C_2 = 15.55$ pF.

When the frequency is above self-resonant frequency, the impedance is capacitive. In the WPT system, the transmitting coil and the receiving coil form an inductive link, so the frequency of the WPT system must be below the self-resonant frequency.

Figure 7 shows the measured and computed ESR R_s as a function of frequency f. AC resistances (23), self-resonant frequencies, inductances and stray-capacitance of the coils are used to calculate R_s. For both coils, when frequency is higher than self-resonant frequencies, error increases dramatically as the frequency increases and measured data becomes very unstable. This is due to the limitation of the model in Fig. 6(a), which is based on the first self-resonant frequency of the coil. So electrical properties of both coils are not in agreement with this model when frequency is much higher than first self-resonant frequency.

Figure 8 shows the measured and computed Q as a function of frequency f. Measured Q is obtained by dividing inductive reactance by R_s: $Q = \frac{\omega L_s}{R_s}$, where L_s is measured equivalent series inductance (ESL).

At higher frequencies, the measured Q values are lower than calculated ones, especially in the $N_T = 56$ case. This is caused by the deviations between calculated inductance values and measured ones, which increase as the frequency becomes higher. Since the calculated inductance values are bigger than measured ones, the calculated Q values become bigger than measured ones. However, for the coil

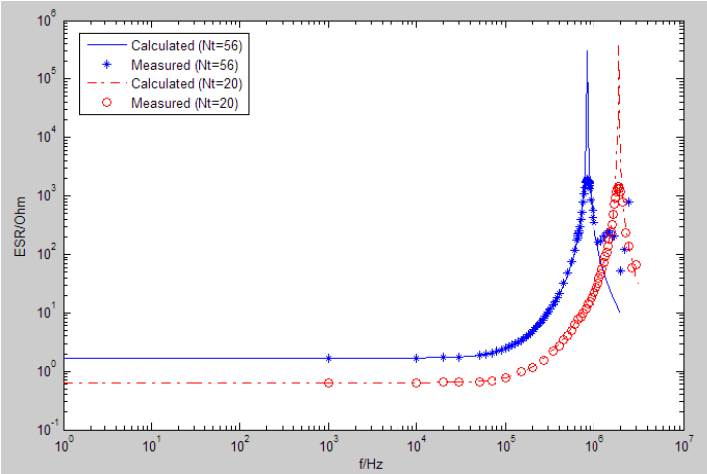

Figure 7. Measured and computed ESR R_s of both coils ($N_T = 56$ and $N_T = 20$) as a function of frequency f.

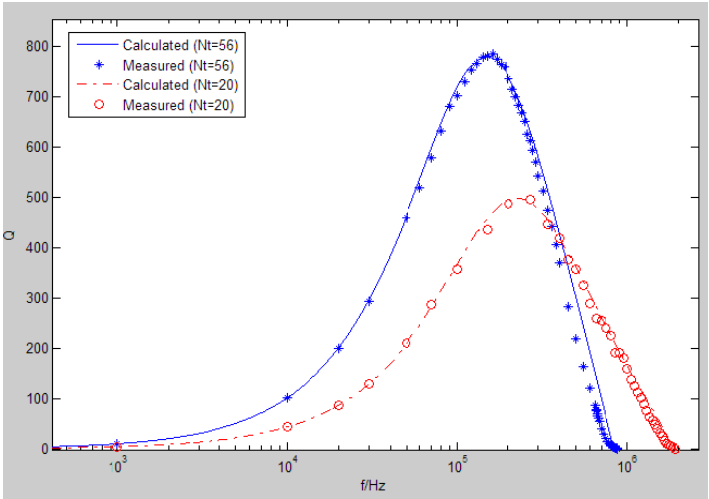

Figure 8. Measured and computed quality factor of both coils ($N_T = 56$ and $N_T = 20$) as a function of frequency f.

with 20 turns, smaller deviations in calculated and measured inductance values result in a less obvious phenomenon. On the other hand, both inductance and resistance values of the 20 turns coil are smaller than those of the coil with 56 turns, while the accuracy of the LCR meter is constant in this particular measurement range. So for lower turns, errors in measured ESL data are larger, thus will cause greater discrepancy in the frequency range around peak Q value.

5. CONCLUSION

In this paper, an analytical expression of the AC resistance of a single-layer air-core Helmholtz coil wound by using litz-wire has been derived. This expression is based on the analytical expression for the AC resistance of solid round wire winding and has taken the magnetic field distribution across winding space into consideration. The accuracy of expression has been verified by comparing the calculated results with experimental results. The theoretical results were in agreement with measured ones when frequency is below the self-resonant frequency of the coil.

REFERENCES

1. Van Gossum, A. and M. Ibrahim, "Video capsule endoscopy: What is the future?," *Gastroenterol. Clin. North Am.*, Vol. 39, 807, 2010.
2. Shiba, K., A. Morimasa, and H. Hirano, "Design and development of low-loss transformer for powering small implantable medical devices," *IEEE Trans. Biomed. Circuits Syst.*, Vol. 4, 77–85, 2010.
3. Ma, G. Y. and G. Z. Yan, "Wireless powered microrobot for gastrointestinal detection," *ICMA'07: Int. Conf. on Mechatronics and Automation*, 1085–1089, 2007.
4. Chen, C. J., T. H. Chu, C. L. Lin, et al., "A study of loosely coupled coils for wireless power transfer," *IEEE Transactions on Circuits and Systems II: Express Briefs*, Vol. 57, No. 7, 536–540, 2010.
5. Chen, L., S. Liu, Y. C. Zhou, et al., "An optimizable circuit structure for high-efficiency wireless power transfer," *IEEE Transactions on Industrial Electronics*, Vol. 60, No. 1, 339–349, 2013.
6. Bartoli, M., N. Noferi, A. Reatti, and M. K. Kazimierczuk, "Modeling litz-wire winding losses in high-frequencies power inductors," *Proc. IEEE Power Electronics Specialists Conf.*, 1960–1966, Baveno, Italy, Jun. 24–27, 1996.
7. Ferreira, J. A., "Analytical computation of AC resistance of round and rectangular litz-wire windings," *IEE Proc. B, Electr. Power Appl.*, Vol. 139, No. 1, 21–25, 1992.
8. Tourkhani, F. and P. Viarouge, "Accurate analytical model of winding losses in round litz wire winding," *IEEE Trans. Magn.*, Vol. 37, No. 1, 538–543, 2001.
9. Nan, X. and C. R. Sullivan, "An equivalent complex permeability model for litz-wire windings," *IEEE Trans. Ind. Appl.*, Vol. 45, No. 2, 854–860, 2009.
10. Wojda, R. P. and M. K. Kazimierczuk, "Winding resistance of litz-wire and multi-strand inductors," *IET Power Electronics*, 2012, Vol. 5, No. 2, 257–268, 2012.
11. Wojda, R. P. and M. K. Kazimierczuk, "Analytical optimization of solid–round-wire windings," *IEEE Transactions on Industrial Electronics*, Vol. 60, No. 3, 1033–1041, 2013.